



Low-temperature silica-rich gold mineralization in mafic VMS systems: evidence from the Troodos ophiolite, Cyprus

Andrew J. Martin^{1,2} · Iain McDonald¹ · Katie A. McFall¹ · Christopher J. MacLeod¹ · Hazel M. Prichard¹

Received: 30 September 2019 / Accepted: 20 July 2020 / Published online: 29 July 2020
© Springer-Verlag GmbH Germany, part of Springer Nature 2020

Abstract

The Troodos ophiolite Cyprus hosts the on-land analogue for actively forming mafic, Cu-rich, or Cyprus-type VMS deposits. In addition to high-temperature (> 350 °C) sulfide mound-related mineralization, other fossil seafloor mineralizing systems are known to operate, including those characterized by an enrichment in Au and abundant silicification. In this study the mineralogy and geochemistry of four Au and silica-rich localities in Troodos are considered, and these include Kokkinovounaros, Mathiatis South, Touronjia, and Alpen Rose. We present whole rock geochemical and mineralogical data characterizing the distribution of Au in the hydrothermal systems of Troodos. Samples from silica-rich localities have two distinct sample mineralogies: supergene samples that contain predominantly goethite, hematite, and jarosite and hypogene samples that contain quartz, amorphous silica and minor hematite. Hypogene samples from Mathiatis South and Kokkinovounaros are enriched in Au with a median concentration of 1.5 ppm relative to supergene samples that contain 0.1 ppm ($n = 107$). This indicates that Au enrichment occurred on the seafloor and is not solely related to supergene weathering of silica-rich mineralization. We suggest that silica-rich Au mineralization in Troodos formed during the migration of newly formed crust off-axis or as white smokers proximal to known VMS deposits. In silica-rich mineralization that is located distally from known massive sulfide deposits, Au was probably remobilized from shallow crustal reservoirs during the low-temperature fluid flow (100–300 °C) in the lower extrusive sequence as the crust cooled and migrated off-axis. Based on modern seafloor analogues, we propose a revised model for the Troodos hydrothermal system that explains the distribution of Au in silica-rich mineralization that formed off-axis and postdates VMS formation and in zones proximal to VMS deposits that formed simultaneously as white smoker-type vents. We suggest that silica-rich mineralized zones formed an intermediary between high-temperature (> 350 °C) on-axis VMS deposits and the low-temperature silicification of umbers (< 100 °C).

Introduction

Gold is an element widely associated with seafloor sulfide mineralization in a range of tectonic settings (Hannington et al. 1991; Moss and Scott 2001; Mercier-Langevin et al.

2011; Melekestseva et al. 2017). Volcanogenic massive sulfide (VMS) deposits associated with the Troodos ophiolite are generally Au-poor (Hannington et al. 1998; Mercier-Langevin et al. 2011); however, previous studies have shown that Au may be concentrated in low-temperature (< 100 °C) “off-axis” silicified umbers (Prichard and Maliotis 1998). In these systems silicification postdates VMS formation and formed distally to the spreading axis as the crust cooled and migrated off-axis (Prichard and Maliotis 1998). It remains unclear for how long and how far spatially off-axis hydrothermal circulation remained active in Troodos, as hydrothermal activity is reported for 20–30-km off-axis in active seafloor spreading environments (Honnorez et al. 1981). In active seafloor hydrothermal systems, black smoker vent sites characterize only the active, high-temperature (~350 °C; Von Damm 1995) portion of the hydrothermal system with extinct sulfide accumulations preserved distally but within a few km of the spreading axis. White smokers occur at the margin of the sulfide mound and

Hazel M. Prichard is deceased. This paper is dedicated to her memory.

Editorial handling: T. Monecke

Electronic supplementary material The online version of this article (<https://doi.org/10.1007/s00126-020-01007-2>) contains supplementary material, which is available to authorized users.

✉ Andrew J. Martin
ajmartin@mun.ca

¹ School of Earth and Ocean Sciences, Cardiff University, Cardiff UK

² Department of Earth Sciences, Memorial University of Newfoundland, St. John's Canada

discharge lower-temperature fluids (250–300 °C; Humphris and Cann 2000) and are enriched in Au, Zn, and Pb relative to black smoker vents (Webber et al. 2017).

Previous studies have identified areas distal to VMS occurrences that contain elevated Au concentrations (> 1 ppm) associated with silicified Mn- and Fe-rich umbers (Prichard and Maliotis 1998). The addition of silica, usually in an amorphous form in umbers which occurred on the seafloor, is fault controlled and locally pervasive over a few meters (Prichard and Maliotis 1998). Gold concentrations in un-silicified umbers were found to average just 5 ppb, whilst silicified umbers contained elevated Au concentrations of up to 5.3 ppm (Prichard and Maliotis 1998). This demonstrates that the circulation of Au- and Si-rich fluid postdates umber formation and is associated with late-stage faulting that occurred in an off-axis position (Prichard and Maliotis 1998).

In this study we investigate a mineralization style that is silica-rich and sulfide-poor that occurs both distally to known VMS deposits and as discrete pods within a few meters of known massive sulfide outcrops. Four localities are considered that display different mineralogical, morphological and geochemical characteristics compared to a typical Troodos VMS deposit. Studies by Prichard and Maliotis (1998) have indicated that Au enrichment is associated with silicification in umbers, however, the temperature and source of Au-rich fluids in these systems remains poorly constrained. This study aims to characterize the source, distribution, and enrichment of Au in VMS deposits and silica-rich mineralized zones of the Troodos ophiolite to better understand the influence of decreasing fluid temperature on Au mobility during the migration of the crust away from the ridge axis.

Geological background

The Troodos ophiolite

The exceptionally exposed Late Cretaceous (~92 Ma; Mukasa and Ludden 1987) Troodos ophiolite of Cyprus hosts the type locality for Cyprus-type, mafic or Cu-Zn VMS deposits (Hannington et al. 1998; Galley et al. 2007; Adamides 2010). The exact tectonic origin of the Troodos ophiolite remains controversial, and it is now widely accepted that Troodos formed in a supra-subduction environment, most likely a nascent fore-arc type setting (Miyashiro 1973; Pearce and Robinson 2010). The domical uplift of Troodos has led to the exposure of a complete oceanic pseudostratigraphy with the mantle section surrounded radially by cumulate and plutonic rocks; the sheeted dyke complex (SDC); the extrusive sequence, consisting of a transitional Basal Group horizon (BG) between the SDC and lavas; and

the upper and lower pillow lavas (UPL-LPL) (Gass 1968, 1980; Fig. 1).

The SDC are locally altered to greenschist facies alteration assemblages (e.g., epidote) indicating high-temperature (> 350 °C) fluid-rock interaction during hydrothermal alteration (Gass and Smewing 1973). Moreover, it is widely accepted that the SDC contributed metals to the overlying hydrothermal system during VMS deposit formation (i.e., spilite and epidosite formation; Jowitt et al. 2012; Patten et al. 2016, 2017).

The spreading structure of Troodos suggests crustal accretion akin to processes recognized at intermediate to slow-spreading ridges (Escartín and Canales 2011). The formation of regional-scale graben structures indicate tectonic stretching, thinning, and rotation of the upper crust during seafloor spreading (Varga and Moores 1985; Fig. 1). Three regional-scale grabens that are thought to represent fossil seafloor spreading ridges are preserved on the northern flank of Troodos (Varga and Moores 1985; Fig. 1). From west to east, these are Solea, Mitsero, and Larnaca grabens. Spreading relationships between grabens suggest that both Solea and Mitsero could have formed in an “off-axis” position, i.e., through the faulting of older crust in a ridge flank-type setting (Hurst et al. 1994; van Everdingen and Cawood 1995). Volcanogenic massive sulfide deposits and silicified umbers are spatially associated with these seafloor structures (Constantinou and Govett 1973; Prichard and Maliotis 1998).

We present four in detail localities that display variable mineralization styles, all of which are distinctly different from VMS deposits. Whole rock Au concentrations for 10 VMS deposits across Troodos are also presented for comparison (ESM 1, Table S1). Samples presented in this study are divided into VMS deposits and silica-rich mineralization. The VMS deposits considered span the entire Troodos ophiolite and contain a full suite of ore types; thus, they are representative of a broad range of physicochemical processes (Martin et al. 2019).

Alpen Rose

Alpen Rose is a northwest-southeast striking ridge forming a prominent topographic high in eastern Troodos, east of the Mathiatis North VMS deposit (Figs. 1 and 2). Alpen Rose is situated in the extrusive sequence, surrounded by 3–10-m wide near vertical dykes that cross-cut subhorizontal pillow lavas. The ridge is quartz-rich containing a breccia unit cross-cut by quartz veins (Figs. 2 and 3). The southern side of the ridge forms a prominent near vertical scarp that increases in height to the east (Figs. 2 and 3).

Structurally Alpen Rose is complex; a fault bound scarp is present on the southern side delineated by a thick unit of breccia (1–3 m) striking parallel to the ridge (Figs. 2 and 3a,b). Rarely, kinematic indicators are preserved indicating

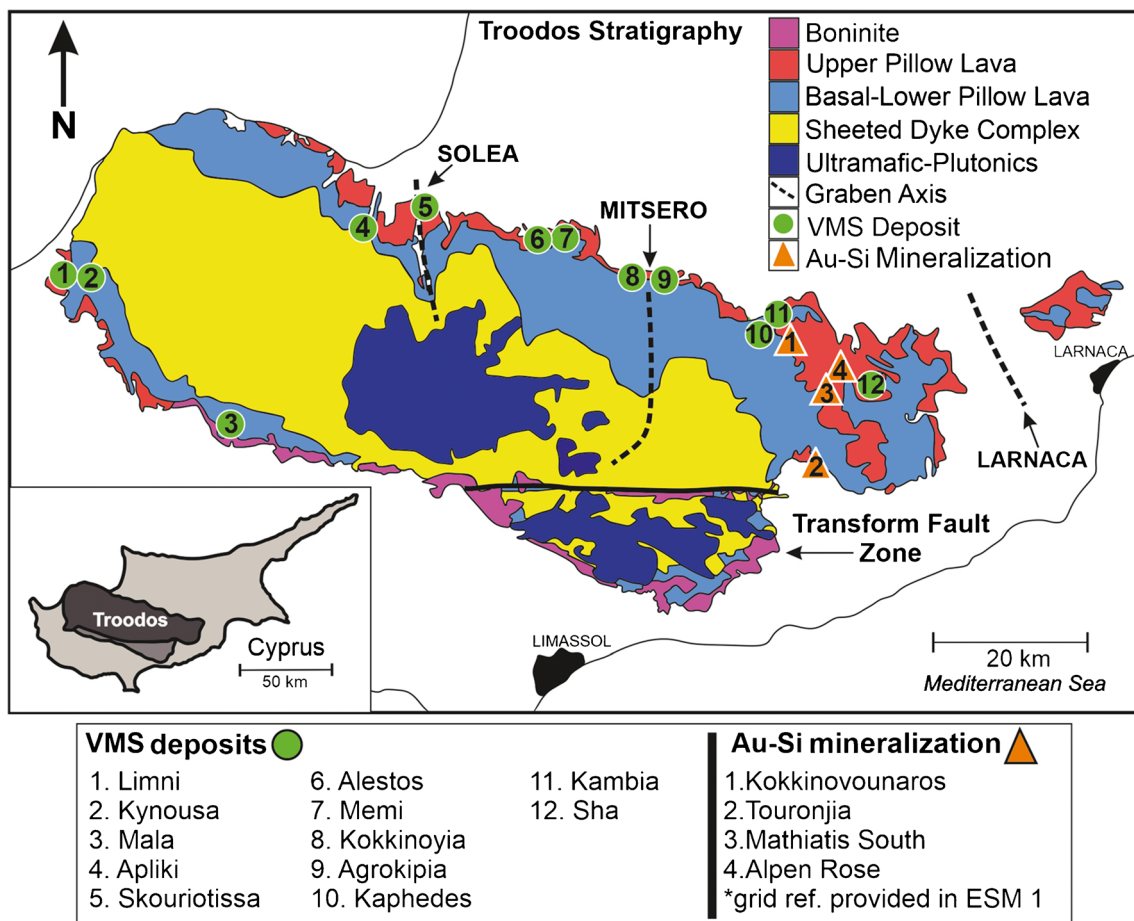


Fig. 1 Simplified geological map of the Late Cretaceous (92 Ma) Troodos ophiolite, Cyprus. Black dashed lines indicate the approximate location of graben axes (after Martin et al. 2019)

an oblique strike-slip sense of movement (Fig. 2). Local scale north-south strike-slip faults have subsequently cross-cut and offset the entire ridge and adjacent dykes with a displacement of 1–5 m. There is no unified sense of displacement on cross-cutting faults, and both sinistral and dextral kinematic indicators are preserved, probably representing fault reactivation under different stress regimes. We infer that Alpen Rose is bound to the southeast by a large north-south trending fault as the ridge and quartz breccia unit end abruptly (Fig. 2).

The mineralized zone is dominantly breccia or vein style and quartz-rich (Fig. 3e,f). Textures are consistent with multiple phases of sulfide- and silica-rich mineralization. Only minor un-oxidized pyrite was observed at Alpen Rose; however, hematite, goethite, and jarosite that indicate sulfide oxidation are the most abundant matrix-hosted minerals (Fig. 3g,h). Veins are less-common than breccia and are typically 30–70 cm wide with a laminated morphology (Fig. 3c,d).

Mathiatis South

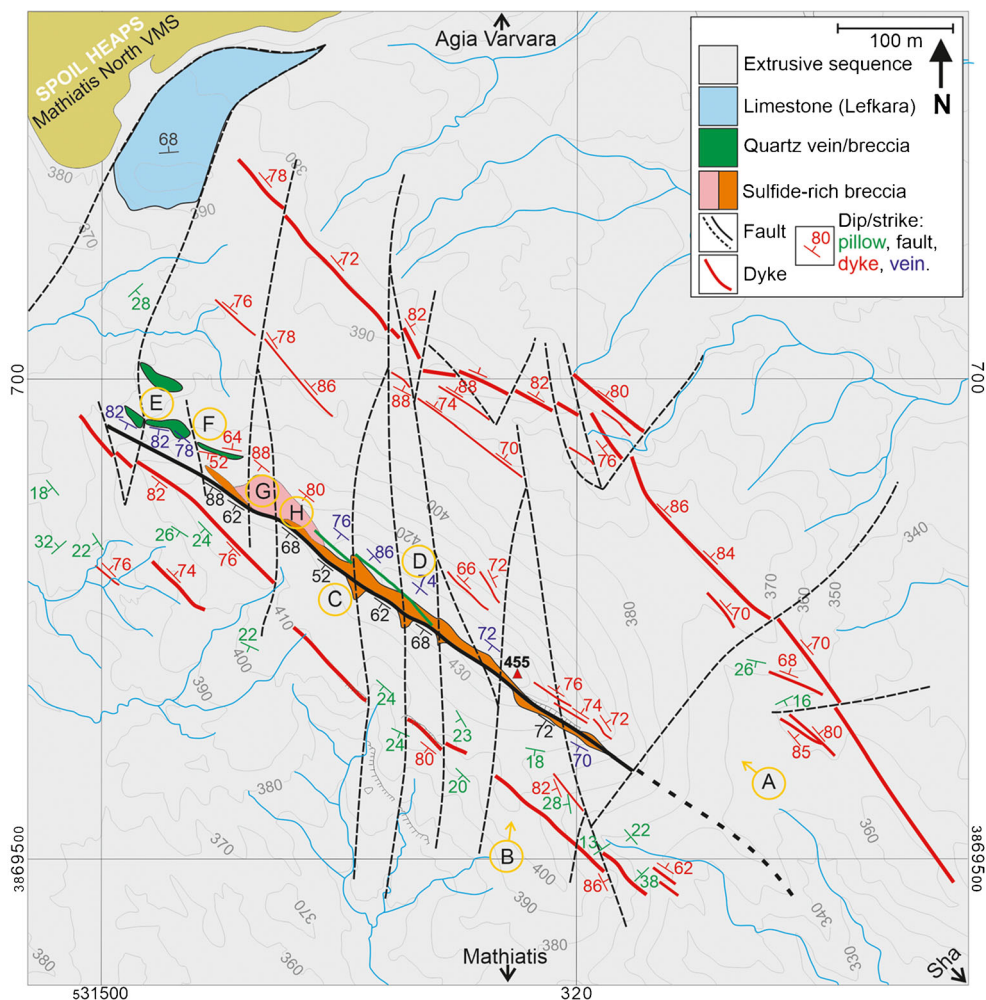
The Mathiatis South deposit has historically been exploited for Au and Cu. It is located southeast of the

village of Mathiatis (ESM 1, Table S1, Fig. 1) and approximately 2.5 km south of the Mathiatis North VMS deposit. The western margin of the deposit contains a Cu-rich massive pyrite lens (Fig. 4a). The center of the open pit is dominated by inter-fingered goethite-, hematite-, jarosite-, and limonite-rich zones with distinct zones of silica-rich brecciated material (Fig. 4c,h). Brecciation is prolific throughout the pit occurring at a range of scales (Fig. 4b–d). In the upper horizon to the east, brecciation becomes less-pronounced instead grading to crudely banded layers (Fig. 4b). Examples of common mineralization styles are summarized in Fig. 4e–h.

Kokkinovounaros

Kokkinovounaros (Red Hill) forms a prominent topographic high 2 km southwest of Analiontas (ESM 1, Table S1, Fig. 1). Altered and mineralized rocks are bound to the east and west by two parallel north-south striking and eastward dipping normal faults (Fig. 5, see map in ESM 2, Fig. S1). Quartz veins and mineralized breccia are traceable along strike for ~500 m and are truncated

Fig. 2 Geological map of Alpen Rose. Where faults are intersected, quartz and sulfide (now Fe-oxide) abundance increases. The surrounding extrusive sequence is cross-cut by a series of dyke swarms (parallel to Alpen Rose) that are truncated by strike-slip faults, indicating that north-south faults postdate northwest-southeast faulting. Letters in yellow circles identify photo localities presented in Fig. 3. See text for further discussion



and offset to the south by a northeast trending fault. The mineralized zone is spatially associated with the north-south faulting with a clear decrease in alteration intensity with distance from the fault plane (~5 m) (Fig. 5a,b). The fault plane is characterized by highly bleached and brecciated lavas with alteration intensity decreasing rapidly from the fault plane to a red-pink zone of jarosite and hematite to a goethite-rich zone at the margins (Fig. 5b).

Brecciation is common throughout Kokkinovounaros with hematite-silica (jasper-rich) breccias occurring proximal to the main north-south fault. Alteration of pyrite is observed as relict cubic pyrite voids now infilled with hematite residue (Fig. 5d). Two different alteration styles are associated with the north-south bounding faults: a stockwork texture that contains disseminated subhedral pyrite (Fig. 5c) and a massive jasper breccia (Fig. 5f-h). Distally from the faults, alteration becomes more chaotic with inter-fingered reds, yellows, whites, and pinks indicating variable amounts of hematite, goethite, silica, and jarosite, respectively. Locally, silicified amber is observed in the hanging wall of faults (Fig. 5e).

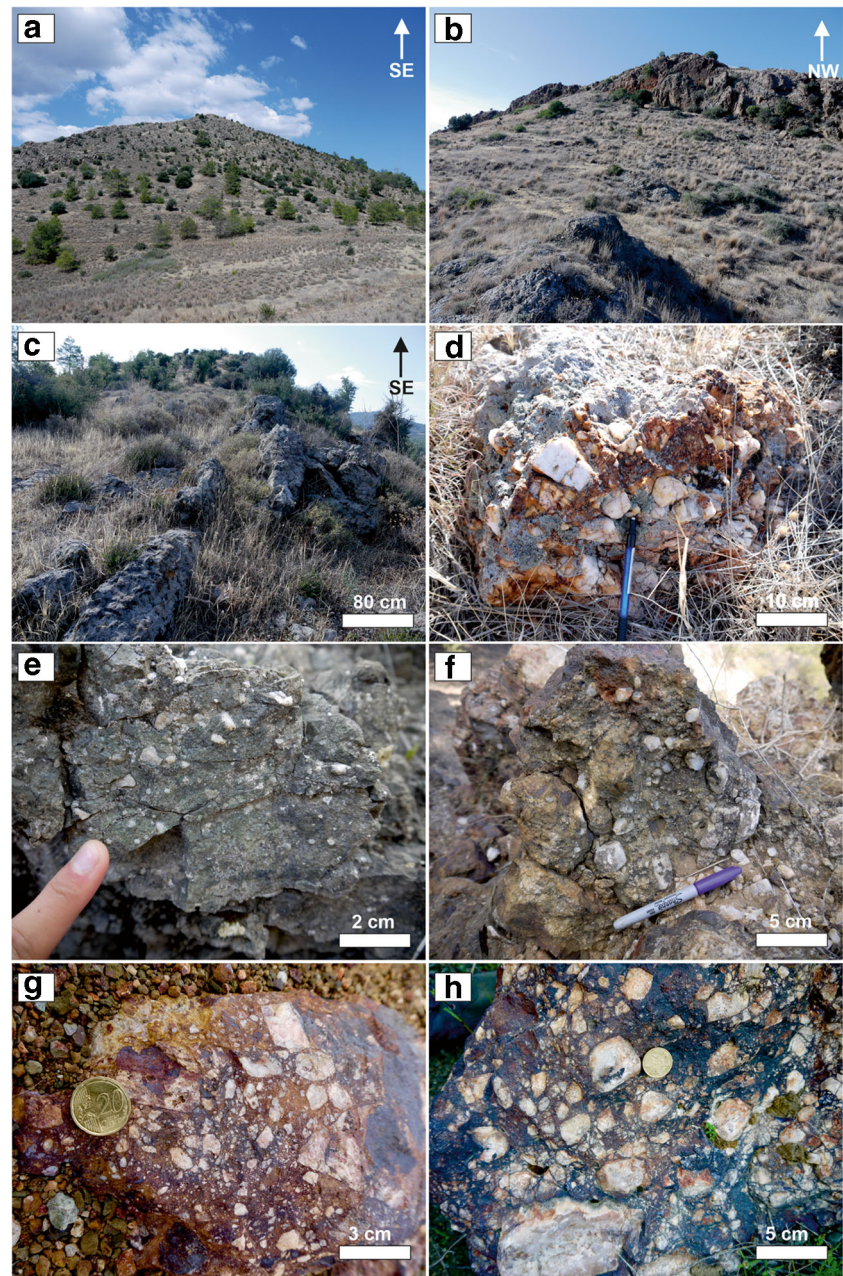
Touronjia

Touronjia is located 3.5 km east-southeast of Kato Lefkara (Fig. 1 and Fig. 6a, ESM 1, Table S1). Silica- and sulfide-rich mineralized BG lithologies grade upwards into LPL flows and brecciated pillows that are directly overlain by the Lefkara limestones (ESM 2, Fig. S2 for summary map). In the lower regions, sinuous crudely sheeted dykes are highly oxidized grading upwards into a bleached gossanous, silica-rich zone where both silicification and minor kaolinization occur (Fig. 6b-f).

The mineralized zone is characterized by pervasive silicification of dykes and pillow lavas accompanied by disseminated pyrite, minor chalcopyrite, and covellite with a brecciated texture (Fig. 6c-h; ESM 2, Fig. S3). Sulfides are associated with silicification in the matrix of breccia units where pyrite is subhedral and occurs as sub mm scale aggregates and disseminations (ESM 2, Fig. S3).

In the uppermost-mineralized horizon, silicification is pervasive, and breccia fragments are hosted in a silica-kaolinite matrix with variable amounts of goethite (Fig. 6a-f). The

Fig. 3 Field photographs from Alpen Rose. **(a)** View looking southeast from the base of Alpen Rose. Alpen Rose forms a prominent topographic high. **(b)** View looking northwest; note the prominent steep sided fault scarp delineating the main breccia zone. **(c)** Top of the main ridge, a massive quartz vein is offset by minor dextral strike-slip faults. **(d)** Quartz breccia vein with silica cement. **(e and f)** Angular quartz clasts in a hydrothermally altered weakly silicified matrix. **(g and h)** Typical hydrothermal “sulfide-rich” breccia. White clasts are sub-angular quartz in a goethite-hematite matrix



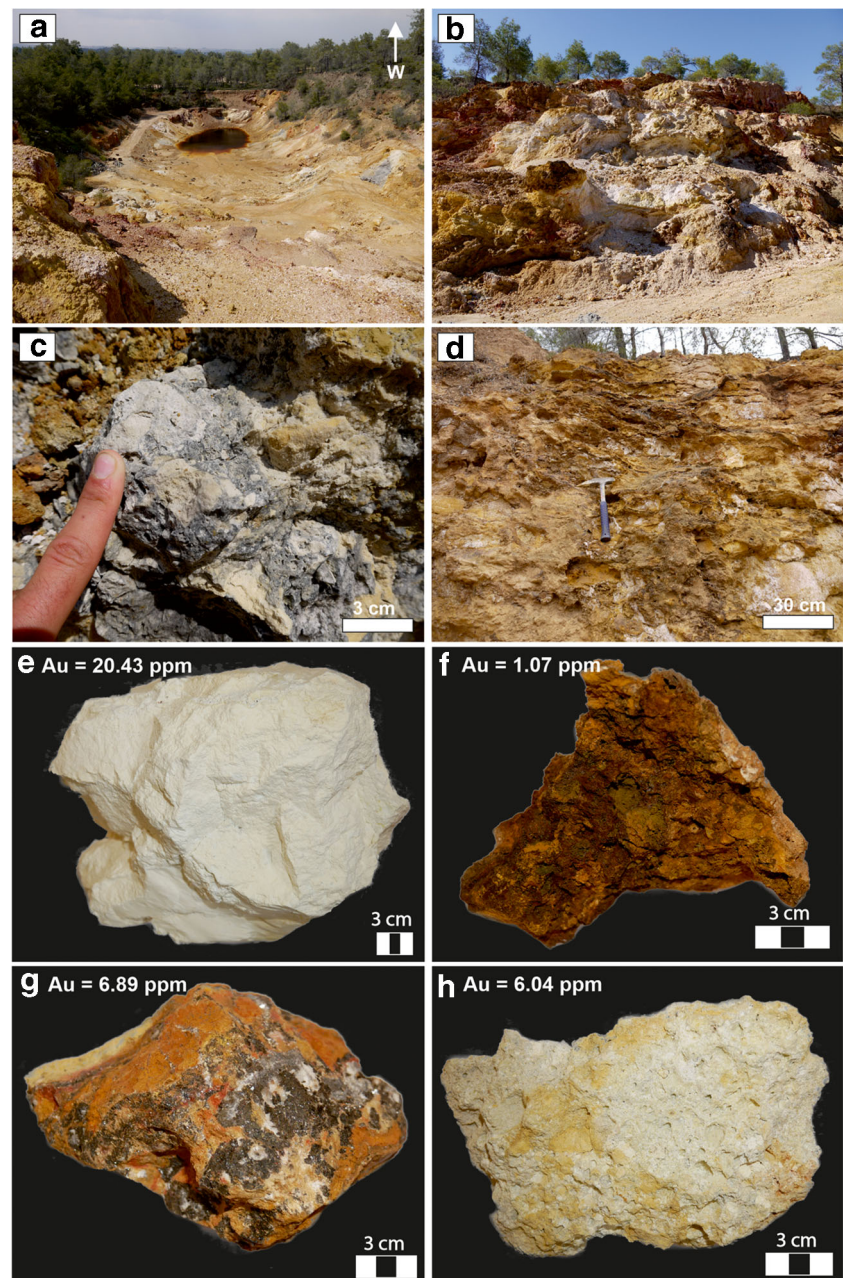
lower regions are less-pervasively silicified and lavas are identifiable (Fig. 6e,f). Veins of goethite, hematite, and silica occur cross-cutting oxidized, but not pervasively altered lavas, and no fresh sulfide is observed (Fig. 6f).

Methods

Whole rock geochemistry was prepared using an aqua regia digest followed by inductively coupled plasma-mass spectrometry (ICP-MS) analysis. Samples were first crushed using a steel jaw crusher followed by pulverization in a tungsten

carbide TEMA mill. Half a gram of sample was then digested using aqua regia (3:1 HCl:HNO₃). 32 ml of HCl and 1.25 ml of HNO₃ were added to the powdered sample and left for 1 h at room temperature for the initial reaction to subside. Samples were then heated at 85 °C for 24 h and left to cool for 1 h. A 1:5 dilution was then performed using MilliQ® 18.2 MΩ de-ionized water ready for analysis. Quantitative trace element analysis was performed at Cardiff University using a Thermo iCAP RQ ICP-MS, and data correction was performed using the Thermo Qtegra software. Standards UM1, CCU1 and SU1A were prepared in the same dilute aqua regia matrix as the unknown samples, RSD values for Au were

Fig. 4 Field photographs from Mathiatis South. (a) View over the historic open pit, note extensive oxidization and acid water lake. (b) Typical gossan exposure, interlayered goethite, jarosite, and hematite. (c) Silica breccia from the main pit. (d) Layered gossan. (e) Silicified lava containing high Au. (f) Typical gossan sample consisting of goethite with minor quartz. (g) Calcite-goethite-rich sample, black mineral is Mn carbonate. (h) Silica breccia exhibiting a “vuggy silica” texture



better than 1.7% (ESM 1, Table S2 and S3). We acknowledge that aqua regia digestion is not capable of total digestion of silicates; therefore, the Au concentrations presented in this study represent minimum values.

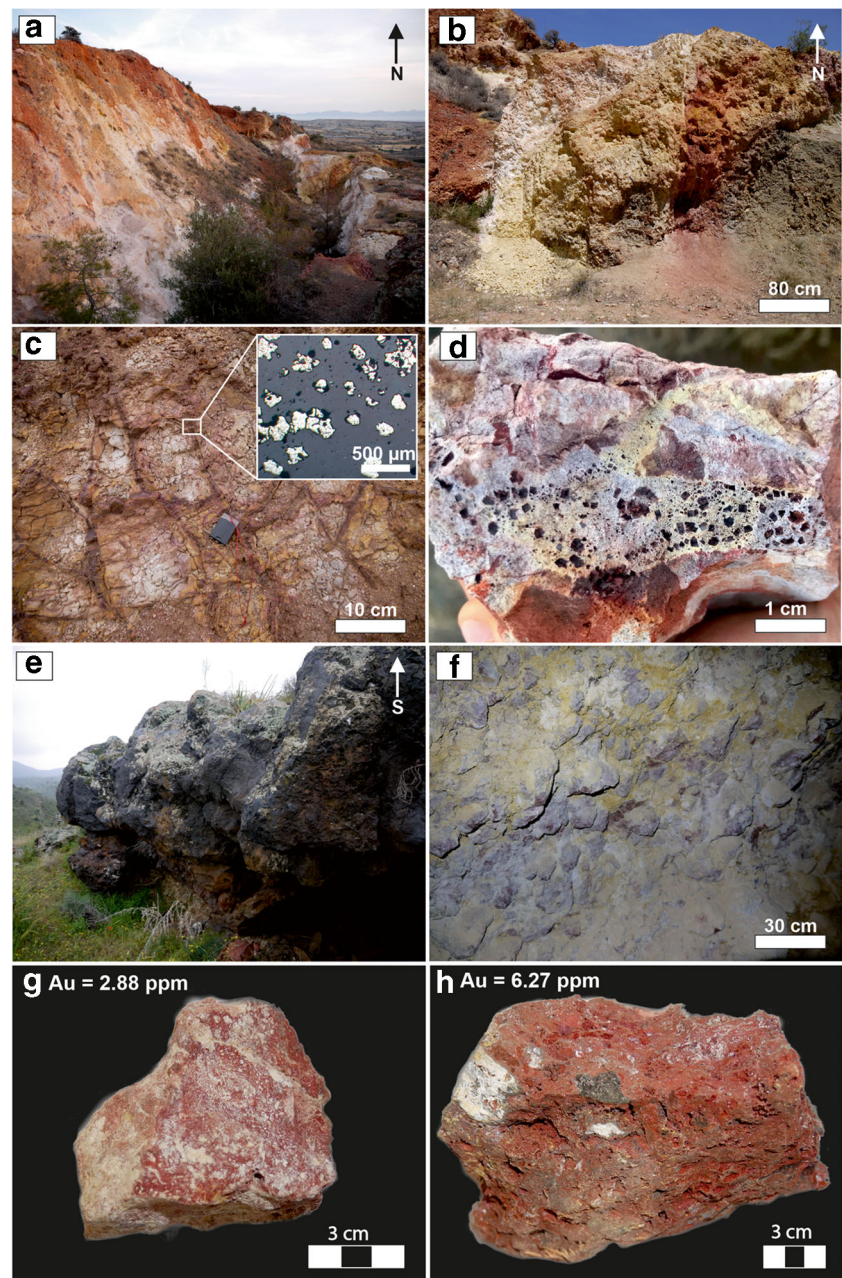
For the identification and quantification of modal mineralogy, X-ray diffraction (XRD) analysis was carried out on powdered samples at Cardiff University. Scans were run using the Philips PW1710 Automated Powder Diffractometer using Cu K α radiation at 35 kV and 40 mA. From the scans, phases were identified using Philips PC Identify software, and from the peak areas, semi-quantitative analysis was performed, and a percentage of each phase present was estimated.

Results

Si-rich sample mineralogy

Modal mineralogy analyzed by XRD is summarized in Fig. 7. Minerals identified include quartz, cristobalite, and amorphous silica and multiple Fe phases including goethite (FeO[OH]), jarosite (KFe³⁺₃[OH]₆[SO₄]₂), hematite (Fe₂O₃), carphosiderite (H₂O•Fe₃[SO₄]₂[OH]₅H₂O), and other minerals including natroalunite (NaAl₃[SO₄]₂[OH]₆), anatase (TiO₂), sergeevite (Ca₂Mg₁₁[CO₃]₉[HCO₃]₄[OH₄•6H₂O]), calcite (CaCO₃), and kaolinite (Al₂SiO₂O₅[OH₄]) (Fig. 7 and ESM 2, Fig.

Fig. 5 Field photographs from Kokkinovounaros. (a) View of the historic open pit (looking north along main pit fault). Note highly bleached lavas surrounding the fault plane. (b) Cross-section of alteration zone surrounding the main pit fault. The fault plane is marked by intense leaching (white) grading through goethite to hematite (orange to red) and finally into “fresh” green-gray pillow lavas. (c) Stockwork veins in close proximity to the western fault, inset image shows subhedral pyrite grains in reflected light. (d) Supergene altered lava: euhedral voids indicate the leaching of pyrite now containing hematite residue. (e) Silicified umber to the south of the main pit exposure. (f) Exposure in a small adit to the north of Kokkinovounaros preserving hypogene jasper-rich breccia mineralization (see ESM 2, Fig. S1). (g and h) Examples of high-Au jasper from location (f) (adit)

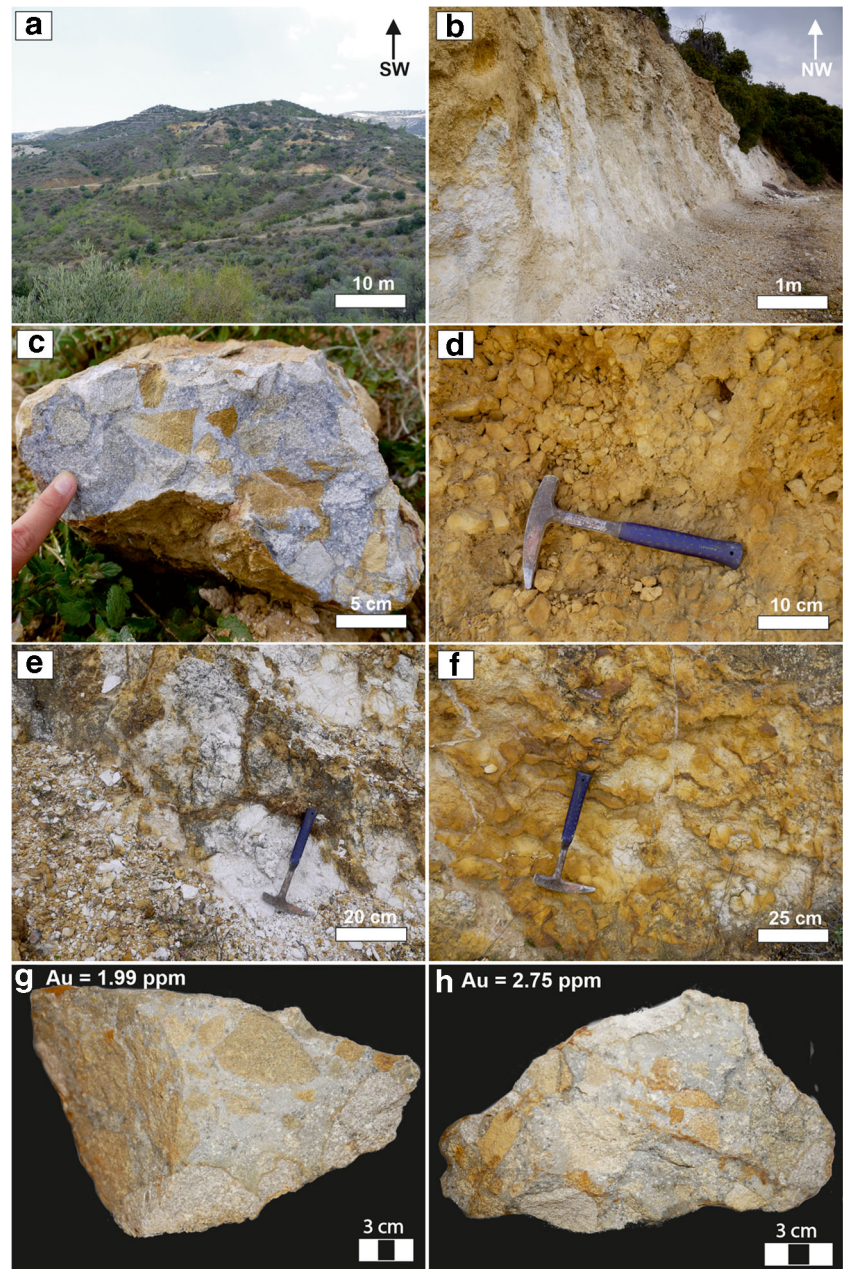


S4). Quartz is the most common mineral occurring in 19 out of 24 of samples analyzed, and its abundance varies significantly from ~5 vol.% to 99 vol.%. Samples from Mathiatis South are the most mineralogically diverse, whilst all other localities analyzed contain predominantly quartz with minor goethite, hematite (Alpen Rose), and kaolinite (Touronjia). Based on XRD analysis and specimen mineralogy, we divide samples from Kokkinovounaros and Mathiatis South into Si-rich, that contain amorphous silica or quartz with only minor hematite and goethite and Fe-rich samples that contain predominantly goethite, hematite, and jarosite with lesser amounts of silica. Full data is available in ESM 2, Fig. S4.

Troodos VMS deposit mineralogy

Samples from 10 VMS deposits were classified based on their sulfide abundance and morphology into massive, semi-massive, disseminated, jasper, stockwork, South Apliki Breccia Zone, ochre, and gossan samples (Fig. 8). Massive sulfide contains > 90% sulfide, mainly pyrite with minor (< 5%) chalcopyrite, and trace sphalerite (< 1%) (Fig. 8a). Semi-massive samples contain < 50% sulfide with a higher silica content (Fig. 8b). Disseminated samples contain fine-grained pyrite (10–20%) but predominantly consist of altered wall rock (Fig. 8c). Jasper samples contain only pyrite (10–20%), hematite, and silica (amorphous or quartz; Fig. 8d). Stockwork

Fig. 6 Field photographs from Touronjia. **(a)** View over the mineralized area, the far hill tops are Lefkara group limestones. **(b)** Upper Touronjia exposure, brecciated highly silicified unit with variable amounts of Fe staining. **(c)** Unweathered surface of Touronjia breccia, the unit is pervasively silicified with trace sulfides. **(d)** Close-up of clast supported Fe-stained breccia. **(e)** and **(f)** Vein hosted “sulfide” mineralization now altered to goethite-jarosite cross-cutting an altered lava. **(g and h)** Examples of high Au samples exhibiting a distinct brecciated morphology with a highly silicified matrix commonly containing disseminated sulfide. See ESM 2, Fig. S2 for photo locations and summary map



samples are characterized by discrete veins of pyrite and chalcopyrite (Fig. 8e). South Apiliki Breccia Zone samples contain high concentrations of chalcopyrite (up to 50%) and variable amounts of covellite, hematite, pyrite, and silica (Fig. 8f; Martin et al. 2018). Ochre samples are finely laminated and contain goethite, jarosite, and minor hematite (Fig. 8g). Gossan samples are typically goethite-rich with a box-work texture (Fig. 8h).

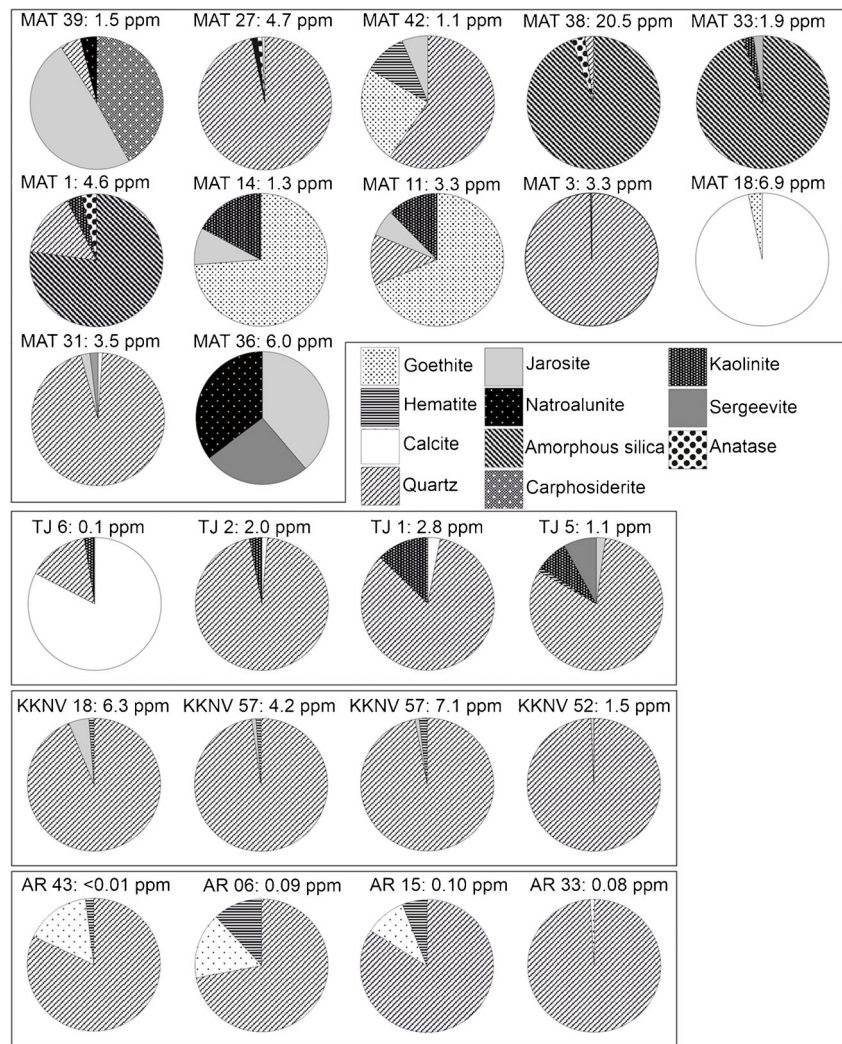
Geochemistry

Of the 166 samples analyzed from silica-rich localities, 25 returned Au concentrations > 1 ppm, with the highest

concentration of 20.43 ppm recorded at Mathiatis South (Fig. 9). Median Au concentrations, independent of sample mineralogy, are 0.02, 0.38, 0.08, and 0.61 ppm ($n = 166$; ESM 1, Table S3) for Alpen Rose, Mathiatis South, Kokkinovounaros, and Touronjia, respectively (Fig. 9). Samples analyzed from Mathiatis South and Kokkinovounaros are sub-divided in Fe- and Si-rich subsets reflecting sample mineralogy.

Of the 48 samples analyzed from Mathiatis South, 15 are Si-rich and 33 are Fe-rich. Gold is notably enriched in Si-rich samples with a median concentration of 1.50 ppm ($n = 15$) compared with 0.24 ppm ($n = 33$) in Fe-rich samples. Silica-rich samples also exhibit an enrichment in Sb, Ag, and Pb and a depletion in Fe, Se, Te, Zn, and As relative to Fe-rich

Fig. 7 Modal mineralogy analyzed by XRD of samples from Mathiatis South (MAT), Touronjia (TJ), Kokkinovounaros (KKNV) and Alpen Rose (AR) (ESM 2, Fig. S4). Samples from Touronjia, Kokkinovounaros and Alpen Rose are quartz dominated with minor Fe minerals whilst Mathiatis South samples are generally jarosite, goethite, and silica-rich (silica* = cristobalite and amorphous phase). Au concentrations of corresponding sample shown above sample in ppm



samples (Fig. 9). Au does not exhibit any notable correlation in Si-rich samples with the exception of silica ($R > 0.5$) (ESM 1, Table S4). Other notable correlations in Si-rich samples include a strong positive correlation between Fe, As, and Se ($R > 0.8$). No notable correlation ($R < 0.3$) exists between Au and other elements analyzed in Fe-rich samples (ESM 1, Table S4).

At Kokkinovounaros, of the 59 samples analyzed, 11 are classified as Si-rich and 48 are Fe-rich. Au is enriched in Si-rich samples with a median concentration of 1.40 ppm ($n = 11$) compared with 0.06 ppm ($n = 48$) in Fe-rich samples (Fig. 9; ESM 1, Table S3). Si-rich samples are highly enriched in Pb and Ag with median concentrations of 8.7 and 68.4 ppm compared with Fe-rich samples at 0.4 and 16.6 ppm, respectively (Fig. 9). Iron-rich samples contained elevated concentrations of Zn, Cu, As, and Mn relative to Si-rich samples. In Si-rich samples, a moderate positive correlation ($R > 0.4$) exists between Au, Mo, and Se, whereas As and Ag have a strong positive correlation ($R = 0.78$; ESM 1, Table S4). A moderate negative correlation is recorded between Au and

Si ($R = -0.6$). In Fe-rich samples, correlation with Au is limited with the exception of a minor positive correlation between Au, Ag, and Sb ($R > 0.3$) (ESM 1, Table S4).

Samples at Alpen Rose contain the lowest median Au concentration at 0.02 ppm ($n = 53$) with only one sample containing > 1 ppm Au. Alpen Rose samples are enriched in Mn and Co relative to all other Si-rich samples (ESM 1, Table S3). Notably, Au exhibits a moderate positive correlation with Fe ($R = 0.65$), whereas in all other deposits, Au and Fe exhibit no correlation ($R = < 0.1$). Additionally, a moderate correlation ($R > 0.6$) is recorded between Au with Ag, As, Sb and Bi (ESM 1, Table S4).

Samples from Touronjia contain median Au concentrations of 0.61 ppm ($n = 6$; Fig. 9). Au exhibits a moderate negative correlation with Si, Fe, Zn, Cu, and Cd ($R = > -0.6$) and a positive correlation with As ($R = 0.77$; ESM 1, Table S4).

The Au content of samples from VMS deposits is highly variable, the highest median Au concentration of 0.26 ppm ($n = 9$) occurs in semi-massive samples followed by ochre at 0.24 ppm ($n = 7$) (ESM 1, Table S5). Jasper, stockwork, and

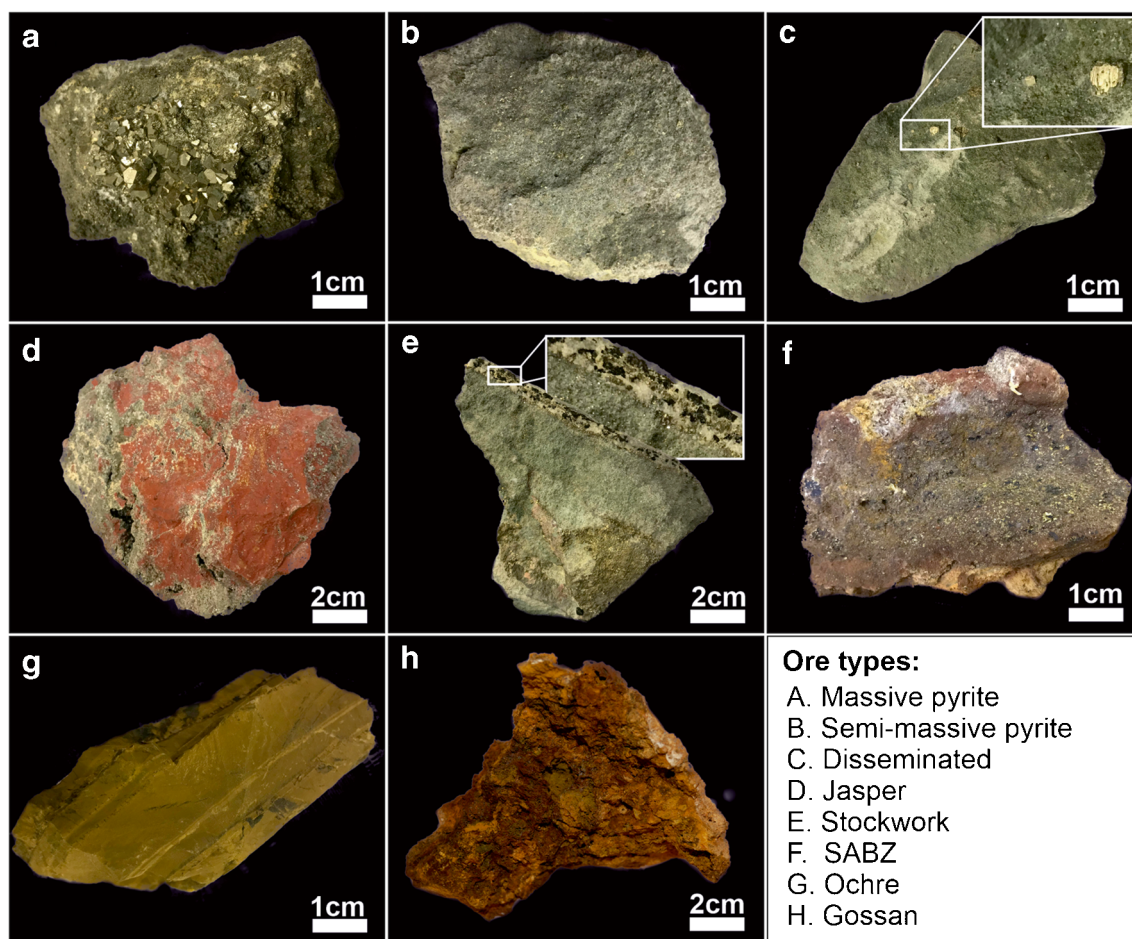


Fig. 8 Examples of ore types analyzed in Troodos VMS deposits. Samples represent different supergene and hypogene processes synonymous with VMS deposits. **(a)** Massive pyrite. **(b)** Semi-massive pyrite with silica. **(c)** Disseminated pyrite in altered lava. **(d)** Jasper with minor disseminated pyrite. **(e)** Stockwork containing chalcopyrite, quartz,

and pyrite-rich veins. **(f)** South Apliki Breccia Zone mineralization consists of a hematite matrix with large quantities of chalcopyrite, covellite, and pyrite. See text for further characterization. **(g)** Ochre containing layered Fe oxides. **(h)** Gossan containing goethite and minor hematite

disseminated samples contained the lowest median Au concentration of 0.02 ppm ($n = 28$). Ochres are enriched in most trace elements relative to massive sulfide samples and contain the highest concentration of Mn, Co, Zn, Se, Ag, and Pb (Fig. 9; ESM 1, Table S5). Correlations between Au and As, Ag, Sb, and Bi are highly variable. Gold exhibits a moderate to strong positive correlation with As, Ag, Sb, and Bi in disseminated samples ($R = 0.6–0.9$; ESM 1, Table S6). The opposite trend is true for ochre samples with a negative correlation between Au, Sb, Bi, and As ($R = -0.2$ to -0.7). See ESM 1, Table S6 for further correlation matrices.

Discussion

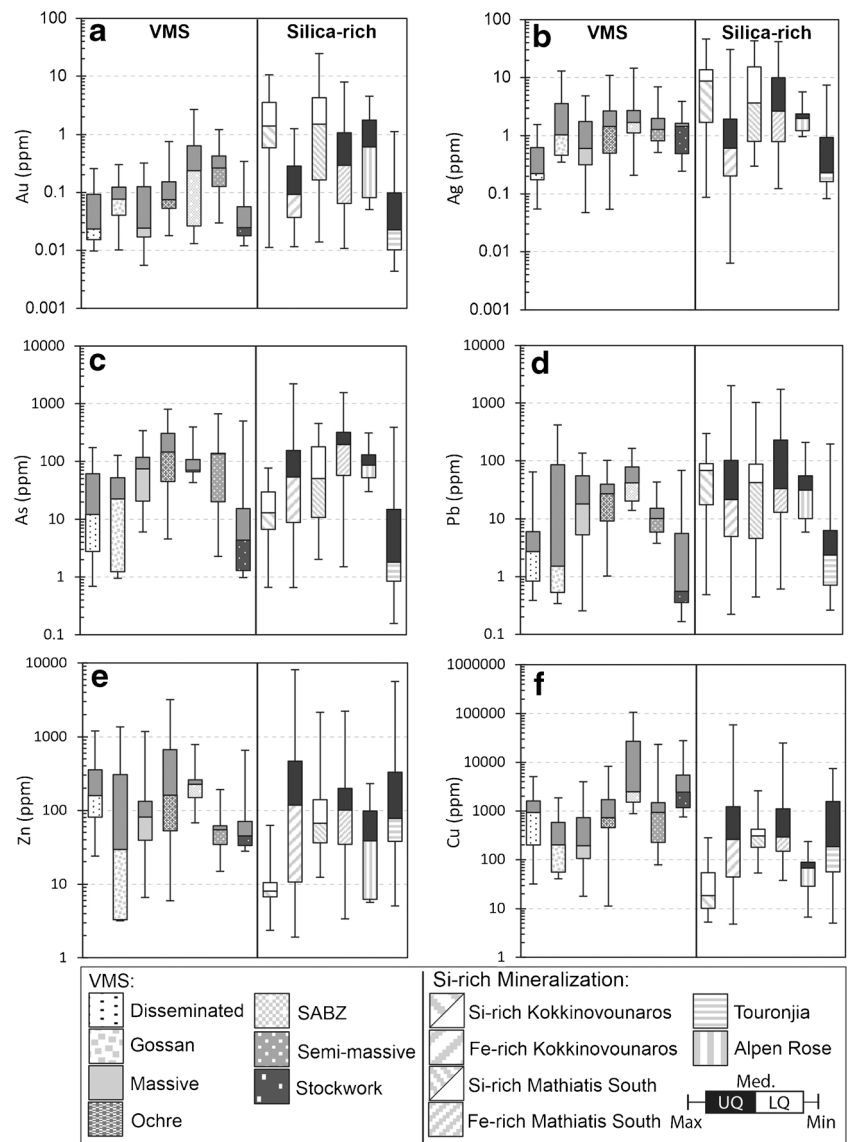
Gold in the Troodos hydrothermal system

Gold is associated with both seafloor and subaerial supergene weathering products of VMS deposits such as gossans and

ochres (Herzig et al. 1991) and hypogene sulfide accumulations such as sphalerite-rich white smoker vents (Urabe and Kusakabe 1990; Gamo et al. 1996; Maslennikov et al. 2017). Mineralogical characterization of samples in this study identified two distinct sample suites, namely, Fe- and Si-rich samples. We suggest that the mineralogical and geochemical differences between Fe- and Si-rich samples represent subaerial supergene and seafloor hypogene processes. Supergene samples contain high concentrations of goethite, jarosite, and hematite (e.g., MAT 39, MAT 36; Fig. 7), common alteration minerals produced by the weathering of sulfide (Herzig et al. 1991), minerals that are notably less-abundant in Si-rich hypogene samples (e.g., MAT 3, KKNV 52; Fig. 7).

At Kokkinovounaros, hypogene samples consist of massive jasper (quartz + hematite) breccias that occur between two north-south trending faults, whilst at Mathiatis South, Si-rich samples occur as discrete silicified pods proximal to massive sulfide. In both instances, the morphology and close spatial association of silicified samples with seafloor faulting

Fig. 9 Whole-rock geochemistry (aqua regia) for low-temperature, silica-rich mineralized zones and VMS deposits classified by location or type morphology (in ppm). (a) Au, (b) Ag, (c) As, (d) Pb, (e) Zn, and (f) Cu. Element correlation is summarized in ESM 1, Table S4 and S6. Upper quartile = UQ, lower quartile = LQ, Med = Median. For full data see ESM 1, Table S3 and S5. For standard information and RSD for all elements, see ESM 1, Table S2



and massive sulfide suggest a seafloor origin. In contrast, the distribution of supergene alteration at Kokkinovounaros and Mathiatis South is widespread showing limited spatial correlation with faults and a decrease in alteration intensity with increasing stratigraphic depth from the exposed weathering surface, further supporting a subaerial supergene origin.

The enrichment pattern of Au differs between supergene and hypogene samples. At Kokkinovounaros median Au concentrations are 1.4 and 0.1 ppm ($n = 59$) for hypogene and supergene samples, respectively. A similar distribution is observed between samples at Mathiatis South where hypogene samples contain median concentrations of 1.5 ppm, whilst supergene samples contain only 0.2 ppm Au ($n = 48$). Furthermore, at both localities the highest Au concentrations correspond to hypogene samples. Thus, the enrichment of Au in Si-rich samples indicates a seafloor origin for Au in Si-rich samples.

In addition to the enrichment of Au in hypogene samples at Kokkinovounaros and Mathiatis South, geochemical distinctions can be made between hypogene and supergene samples, for example, Ag and Pb are enriched in hypogene samples relative to supergene samples (Fig. 9). In contrast, supergene samples may be enriched in As, Se, Cu, and Sb, indicating that these metals were primarily hosted in sulfide minerals (Martin et al. 2019) or were preferentially adsorbed onto Fe(oxy)hydroxides during sulfide oxidation (Balistrieri and Chao 1987; Mamindy-Pajany et al. 2009).

The geochemical signatures of Troodos massive sulfides and hypogene Si-rich samples also differ. Massive sulfide samples from VMS deposits are depleted in Au relative to hypogene samples from Kokkinovounaros, Mathiatis South, and Touronjia (Fig. 9). Additionally, massive sulfide samples are enriched in Cu relative to Si-rich samples with median Cu concentrations across all VMS sample types of 933 ppm ($n =$

70). The difference in geochemistry between massive sulfide- and Si-rich samples can be explained by the affinity of certain metals in high-temperature (~350 °C) and sulfide-rich systems. For example, Cu in stockwork zones (Galley et al. 2007) or the enrichment of intermediate to high-temperature elements such as Bi, Mo, Se, Co, and Te in VMS deposits (Keith et al. 2016; Monecke et al. 2016; Fig. 9). Our data indicates higher median concentrations of Bi, Se, Co, Mo, and Te in VMS samples relative to hypogene Si-rich samples, suggesting that Si-rich samples formed at lower-temperatures (e.g., < 300 °C) (ESM 1, Table S3). This is supported by an enrichment of low-temperature elements such as Pb, Sb, and Au in Si-rich samples relative to Troodos VMS deposits (Huston and Large 1989; Monecke et al. 2016).

The occurrence of lower-temperature fluid venting in Troodos is further supported by fluid inclusion studies at Touronjia (Naden et al. 2006). Mean homogenization temperatures of quartz-hosted fluid inclusions at Touronjia were 209 °C supporting the occurrence of lower-temperature fluid circulation (< 300 °C). Additionally, we apply sphalerite geothermometry (Scott and Barnes 1971; Keith et al. 2014) to the previously published data of Adamides (2013). The application of sphalerite Fe/Zn ratios in this study to data of Adamides (2013) for a Zn-rich prospect located south of Mitsero yield average precipitation temperatures of 246 °C (min = 230 °C, max = 273 °C, $n = 14$), supporting the occurrence of lower-temperature fluid circulation in Troodos. Hannington et al. (1998) also described a bi-modal distribution in sphalerite Fe content in Troodos VMS, possibly indicating the presence of both high- and low-temperature fluids. These low-temperature fluids (< 300 °C) contrast those typical for a Troodos VMS deposit, with Keith et al. (2016) reporting average precipitation temperatures of 411 °C derived from sphalerite at the Skouriotissa VMS deposit. These data indicate that both high-temperature black smoker (> 300 °C; Von Damm 1995) and lower-temperature hydrothermal activity (< 300 °C) were present during seafloor spreading.

White smoker vent complexes in active hydrothermal fields associated with VMS deposits are reported as localized features. For example, the Kremlin area of the TAG mound that is approximately 20–50 m in diameter and situated < 100 m from high-temperature black smoker vents (> 363 °C; Tivey et al. 1995). Increased silica abundance, similar to that observed in hypogene samples from Kokkinovounaros and Mathiatis South and in Touronjia samples is also documented for active white smoker vents with amorphous silica and barite intergrown with pyrite and sphalerite (Koski et al. 1984; Tivey et al. 1995). Similar textural and mineralogical associations have been described for the extinct MESO vent site(s) in the central Indian Ocean that are characterized by jasper breccias that formed at temperatures of < 265 °C (Halbach et al. 2002). Similar mineralogical associations are documented in Troodos silica-rich localities, for example, at Kokkinovounaros where

elevated Au concentrations are associated with jasper-rich breccias (Fig. 5f–h). In combination, temperatures derived from sphalerite geothermometry (Adamides 2013), fluid inclusion analysis (Naden et al. 2006), and indirectly from mineralogical and geochemical variations between VMS deposits and silica-rich mineralized zones in this study indicate different chemical and physical fluid properties between these hydrothermal systems. Fluids responsible for forming silica-rich mineralization in Troodos were relatively low-temperature ~ 250 °C, Au-rich and in some instances where hematite forms the dominant Fe mineral, fluids were locally more oxidizing.

Previous studies at Touronjia by Naden et al. (2006) suggest a possible magmatic volatile source for Au; analogous to processes associated with subaerial epithermal-type mineralization (White and Hedenquist 1990). This observation is primarily based on the occurrence of kaolinite and dickite as key alteration minerals indicating low pH fluids (White and Hedenquist 1990). In their proposed model, Au and associated elements such as Bi, Te, and Se are sourced from the direct contribution of a magmatic volatile phase (Yang and Scott 1996; Heinrich et al. 2004; de Ronde et al. 2005). If this was the case, then an enrichment in these elements is expected at Touronjia, and this is not observed with median concentrations of 0.02 ppm Bi, 0.11 ppm Te, and 1.34 ppm Se ($n = 6$; ESM 1, Table S3). Additionally, fluid inclusion data presented by Naden et al. (2006) yield an average salinity close to modern seawater (~3.5 wt.% NaCl) suggesting fluids of seawater and not magmatic origin (brine or vapor), supporting a low-temperature seawater origin.

The mineralized zone at Alpen Rose shares many similar attributes with other localities, e.g., abundant silicification and brecciation, yet Alpen Rose is depleted in Au compared with other silica-rich localities (median = 0.02 ppm Au, $n = 53$). We suggest that local-scale permeability variations coupled with a high-temperature fluid source (> 300 °C) explain this depletion. Gold at Alpen Rose was probably associated with sulfide minerals as it exhibits a moderate positive correlation ($R = > 0.5$) with Pb, Te, Ag, Mo, and Fe (ESM 1, Table S4); in all other silica-rich samples, a negative correlation with Fe is observed. At Alpen Rose, goethite and hematite are abundant and occur in the matrix of breccias representing the supergene oxidization of pyrite during weathering. Additionally, a small enrichment in Co at Alpen Rose relative to massive sulfide samples and other silica-rich localities could represent a high-temperature fluid source (~350 °C; Keith et al. 2016) with a comparable trace element composition to VMS stockwork samples, excluding Cu that is relatively depleted at Alpen Rose (Fig. 9). We infer that the geochemical signature preserved at Alpen Rose is indicative of fluids that were not affected by later low-temperature off-axis fluid flow, and therefore no Au enrichment occurred (Fig. 10).

This hypothesis is supported by field observations at Alpen Rose that indicate that the majority of quartz formed early in

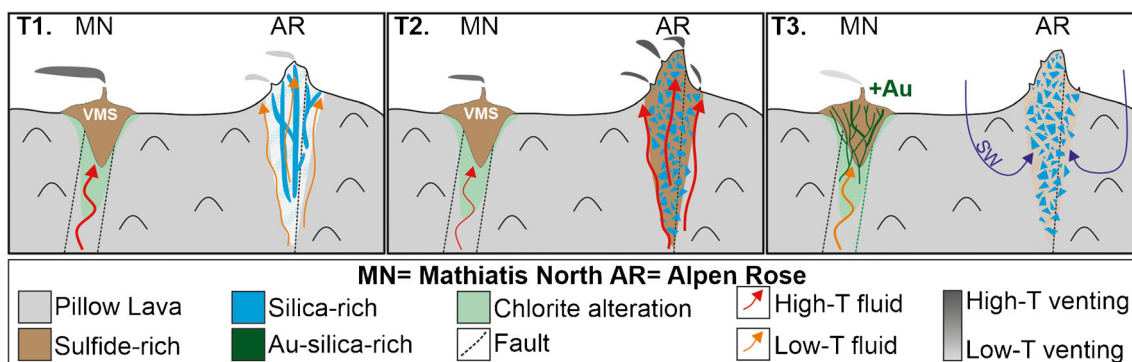


Fig. 10 The formation of Alpen Rose mineralization (MN = Mathiatis North VMS deposit, AR = Alpen Rose). **T1**: Alpen Rose forms proximal to the ridge axis from intermediate temperature silica-rich fluids. At this time, the Mathiatis North VMS deposit forms at the ridge axis. **T2**: Fault movement at Alpen Rose increases permeability leading to

brecciation of early quartz veins and the venting of high-temperature fluids ($> 300\text{ }^{\circ}\text{C}$) that leads to the precipitation of sulfide-rich mineralization. Sulfides occlude fluid flow pathways. **T3**: As the fluid flow at Alpen Rose decreases, late stage off-axis Au- and silica-rich fluids are channeled through the nearby, more permeable Mathiatis North VMS deposit

the deposit paragenesis as it predates sulfide (now goethite-hematite) formation that occurs in the matrix of breccias (Fig. 3g,h). Initial quartz brecciation occurred during a period of increased fault movement that led to a localized increase in permeability facilitating a high-temperature fluid pulse and sulfide precipitation (Fig. 10). The precipitation of sulfides occluded initial permeability pathways, effectively sealing the Alpen Rose hydrothermal system from later, lower-temperature silica- and Au-rich fluids (Fig. 10). These late-stage low-temperature fluids were channeled through the nearby Mathiatis North VMS deposit where late Au-rich quartz veins cross-cut massive sulfide (Martin et al. 2019). This indicates that Au and silicification post-date VMS deposit formation, as demonstrated by Prichard and Maliotis (1998) for silicified umbers. Therefore, the low Au concentrations at Alpen Rose can be explained by (i) the timing of silicification and quartz formation relative to fault movement; (ii) the high-temperature, probably near axis location of Alpen Rose; and (iii) sulfide precipitation leading to the occlusion of late-stage fluid pathways (Fig. 10).

Models for gold enrichment

Silica-rich mineralized zones in Troodos are comparable to a variety of modern day sites of intermediate-temperature ($\sim 250\text{--}300\text{ }^{\circ}\text{C}$) fluid venting that occur within the VMS mound as white smokers or off-axis as sites of diffuse fluid discharge (“shimmering water”; $\sim 50\text{ }^{\circ}\text{C}$) (Hannington et al. 1991; Gamo et al. 1996; Humphris and Cann 2000; Halbach et al. 2002). Silica-rich mineralized zones sampled in Troodos share many similar attributes with seafloor hosted intermediate to low-temperature vent sites, including (i) abundant silica and silicification, (ii) mineralization that occurs distally to high-temperature VMS deposits, (iii) an enrichment in Au,

and (iv) indirect mineralogical and geochemical evidence of lower-temperature fluid flow $< 300\text{ }^{\circ}\text{C}$.

Gold in the Troodos ophiolite was initially mobilized during high-temperature ($> 350\text{ }^{\circ}\text{C}$) fluid-rock interaction within the SDC, as epidosite zones (Fig. 11) that form a source region for some metals in Troodos VMS deposits are depleted in Au (Patten et al. 2017). Upwelling high-temperature ($> 350\text{ }^{\circ}\text{C}$), metal-rich fluids undergo mixing with shallow, low-temperature, oxidized seawater-derived fluids at the BG-LPL boundary (Alt 1994, 1995). Mixing between down-welling seawater and up-welling hydrothermal fluid within this transitional zone facilitates the precipitation of secondary pyrite that incorporates trace metals (Alt 1994; Alt and Teagle 2003). Disseminated pyrite is widely observed throughout the BG-LPL transition in Troodos, most notably in areas such as Almyras and Mosfiloti (Fig. 11).

Secondary disseminated sulfides probably formed at temperatures $< 250\text{ }^{\circ}\text{C}$ as celadonite and chalcidony are the dominant alteration minerals present in the LPL stratigraphy of Troodos (Gass and Smewing 1973; Alt 1994). Disseminated sulfide formed at, or within close proximity to the spreading axis, would have been coeval with high-temperature hydrothermal systems that formed in areas of focused fluid discharge associated with graben bounding faults and VMS deposit formation (Fig. 11). The associated change in redox and decrease in temperature during the diffuse mixing of hydrothermal and seawater derived fluids within the BG in a “near axis” position provide a trapping mechanism for Au and other trace metals that are incorporated into disseminated sulfides (Fig. 11; Alt 1994). In the shallow low-temperature alteration zone (UPL), temperatures were cooler ($< 120\text{ }^{\circ}\text{C}$; Pedersen et al. 2017), and pyrite formation by biogenic sulfate reduction could have occurred; however the extent of this process in Troodos is poorly constrained (Alt and Shanks 2011;

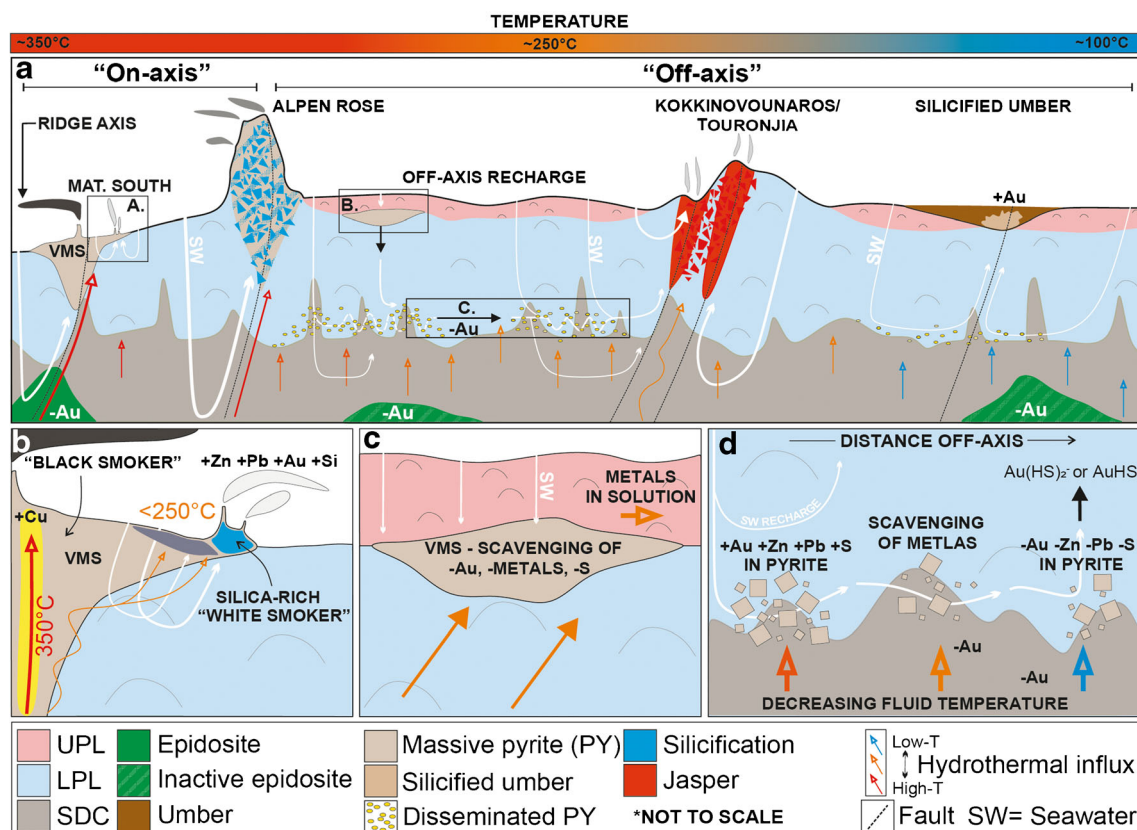


Fig. 11 (a) Schematic summary of the enrichment of Au in the Troodos hydrothermal system. Gold is initially sourced from leaching of metals in the SDC. In close proximity to the ridge axis Au may be enriched in white smoker mineralization. (b) Gold in a white smoker-type setting, e.g., Mathiatis South. The enrichment of Au reflects mound scale fluid flow, and Au enrichment is spatially associated with massive sulfide accumulations. Slightly further off-axis but still within an area of high heat and fluid flux Alpen Rose forms (Fig. 10). (c) Gold may be sourced through leaching of metals from VMS deposits. Lower-temperature hydrothermal fluid (orange arrows; 100–300 °C) remobilizes and scavenges trace metals from sulfides in the VMS mound. (d) Diffused

fluid flow from the underlying SDC mixes with circulating seawater leading to the precipitation of disseminated sulfides within the BG-LPL stratigraphy (orange arrows). As the fluid flow and heat flux decrease as the crust migrates further off-axis fluid become progressively cooler (< 300 °C) and metals are scavenged and remobilized from sulfide minerals (mainly pyrite) by lower-temperature fluids. Gold is transported as sulfide and bisulfide complexes. Fluids are then channeled along late-stage reactivated faults leading to the formation of silica-rich Au mineralization. The silicification of umber occurs distally at temperatures of ~100 °C as the crust continued to migrate off-axis and fluids cooled further

Pedersen et al. 2017). Patten et al. (2016) document elevated concentrations of Au, As, Sb, and Se in sulfides at the transitional zone between the SDC and overlying pillow lavas in Hole 1256D (Cocos Plate). They suggested that the mixing of hydrothermal fluids with seawater at this horizon acted as a sink for trace metals that were mobilized during epidosite formation and the alteration of the SDC below (Fig. 11; Patten et al. 2016).

As the crust migrated further from the ridge axis, heat and fluid flux from the underlying SDC decreased, whereas the amount of seawater influx remained high leading to a decrease in fluid temperature distally (km's to 10's of km) from the spreading axis (Alt 1995; Alt and Teagle 2003). In contrast to high-temperature on-axis VMS forming fluids, the cooler off-axis fluids (< 300 °C) effectively scavenged and remobilized metals that have an increased affinity for lower-

temperature fluids such as Au, Zn, Pb, and Sb (Monecke et al. 2016) from BG sulfides, earlier formed VMS deposits, and inactive epidosite zones (Fig. 11; Hannington et al. 1986). Gold will be transported as sulfide or bisulfide complexes more efficiently in these lower-temperature fluids (Williams-Jones et al. 2009; Pokrovski et al. 2014). Low Au concentrations at Alpen Rose and VMS deposits in Troodos are attributed to the decreased solubility of Au at high-temperatures (~350 °C) where neither Cl^- nor HS^- complexes effectively transport Au (Hannington and Scott 1989; Williams-Jones and Heinrich 2005; Williams-Jones et al. 2009; Pokrovski et al. 2014). We propose that Touronjia, Kokkinovounaros, and Alpen Rose represent an intermediary (~250 °C?) between a typical high-temperature (> 350 °C) VMS deposit and the low temperature < 100 °C silicification of umber (Fig. 11) (Prichard and Maliotis 1998).

Alternate processes where Au is enriched through the addition of a magmatic volatile phase have been suggested for VMS deposits in bi-modal environments (Yang and Scott 1996; Sun et al. 2004; Patten et al. 2019). However, our data provides little evidence of magmatic dominated fluids in silica-rich mineralized zones, for example, the lack of an advanced argillic alteration assemblage (e.g., natroalunite, pyrophyllite, and native sulfur) that indicate low pH, magmatic volatile-rich fluids (Herzig et al. 1998; de Ronde et al. 2019). We also suggest that if a magmatic volatile influx did occur in Troodos, it would have been limited to high-temperature hydrothermal systems in an on-axis position and the initial stages of VMS deposit formation and not off-axis regions (Martin et al. 2020).

At Mathiatis South, Au enrichment reflects local-scale processes related to zone refining and mound-scale fluid flow and not the remobilization of Au during off-axis fluid flow. At Mathiatis South, Au was remobilized from the high-temperature inner core zone of the VMS mound towards the cooler mound margins during zone refining (Galley et al. 2007). This resulted in the simultaneous venting of high- and intermediate-temperature fluid, similar to actively forming black and white smoker complexes (Fig. 11), such as the Kremlin area of the TAG mound (Humphris et al. 1995; Petersen et al. 2000). All other localities investigated are located distally to known VMS deposits and do not reflect mound-scale remobilization processes. If this were the case, then Au would not demonstrate a clear association with quartz veins that cross-cut and postdate VMS formation, for example, at the Mathiatis North VMS deposit (Martin et al. 2019).

Further detailed investigation to quantify and validate the proposed model should include the detailed petrographic and geochemical analysis of sulfides and oxides from the BG transition zone. This should be complimented by sulfur isotope analysis ($\delta^{34}\text{S}$) of sulfides from silica-rich mineralized zones to elucidate a magmatic volatile source of metals in the off-axis hydrothermal system.

Structural implications

All silica-rich mineralized zones investigated in this study are structurally controlled and occur in the eastern portion of the Troodos ophiolite in a complex region known as the Makheras domain (Varga and Moores 1985). The Makheras domain is bound by the Larnaca graben to the east and the Mitsero graben to the west. Throughout the area, northwest-southeast and north-south faulting is observed. The intersection of these two fault directions appears to be important in controlling the distribution of Au and silicification in off-axis mineralized zones.

Low-temperature silica-rich mineralized zones are spatially associated with either normal or strike-slip faulting. The Makheras structural domain (cf. Varga and Moores 1985) exhibits cross-cutting relationships consistent with multiple, temporally distinct faulting and hydrothermal events. For example, at Alpen Rose where northwest-southeast trending faults and dykes are cross-cut by strike-slip north-south trending faults. This indicates that axial parallel northwest-southeast trending faults (Larnaca) were cross-cut by later re-activated faults associated with the north-south orientated Mitsero graben. The interplay between these two structural regimes relates to the migration of spreading between different ridge axes that led to localized dilation, reactivation, and propagation of new faults aligned to the developing stress regime in an off-axis position. Renewed faulting in older, cooler, and more permeable crust by late-stage cross-cutting faults likely acted as a conduit channeling late-stage silicifying fluids (Prichard and Maliotis 1998), and similar cross-cutting fault regimes have been identified at Touronjia and Kokkinovounaros.

Summary and conclusions

Silica-rich mineralized zones in Troodos form an intermediary between on-axis VMS deposits ($>350\text{ }^\circ\text{C}$) and the low-temperature silicification of umbers ($<100\text{ }^\circ\text{C}$). Geochemical data identify an enrichment in Au at Kokkinovounaros, Mathiatis South, and Touronjia relative to Troodos VMS deposits. Zones of silica-rich mineralization at these localities share common attributes including their geochemistry and abundant quartz or amorphous silica. We draw parallels between silica-rich mineralized zones in Troodos and active white smoker or diffuse vents on the modern seafloor. Low-temperature mineralized zones are variably enriched in Au, Sb, Pb, and Zn relative to Troodos VMS deposits. This enrichment reflects the enhanced solubility of these metals in low to intermediate-temperature fluids ($\sim 100\text{--}300\text{ }^\circ\text{C}$) that were generated either at the margin of the VMS mound as white smokers (e.g., Mathiatis South) or during the migration of crust away from the spreading axis (e.g., Kokkinovounaros).

As the crust migrated away from the spreading axis, fluids became progressively cooler. These lower-temperature fluids ($100\text{--}300\text{ }^\circ\text{C}$) transported Au more effectively as sulfide and bisulfide complexes. In off-axis mineralization, we suggest that Au was scavenged and remobilized from BG sulfides or epidote zones. These Au-rich fluids were then channeled along reactivated faults at graben margins in an off-axis position concentrating fluid flow leading to the formation of Au- and silica-rich mineralized zones. Our data also indicates that intermediate-temperature fluid flow ($\sim 250\text{--}300\text{ }^\circ\text{C}$), possibly

as white smokers, formed on-axis in close proximity to massive sulfide deposits. In these areas, Au is locally remobilized during zone refining of the sulfide mound.

Acknowledgments The authors acknowledge the support of the Geological Survey Department of Cyprus, especially Costas Constantinou and Andreas Zissimos. We thank Michael Green, Lazaros Georgiou, and Ifigenia Gavriel for discussion and assistance in the field. Anthony Oldroyd is thanked for his assistance during XRD analysis. This research was funded by the NERC SoS consortium grant NE/M010848/1 “TeaSe: tellurium and selenium cycling and supply” awarded to Cardiff University. We thank Clifford Patten and an anonymous reviewer for their comments that greatly improved this manuscript. We also thank associate editor Thomas Monecke and the editor-in-chief Georges Beaudoin for the efficient editorial handling of the manuscript. We dedicate this manuscript to the late Hazel M. Prichard.

References

- Adamides N (2010) Mafic-dominated volcanogenic sulphide deposits in the Troodos ophiolite, Cyprus part 2- a review of genetic models and guides for exploration. *Appl Earth Sci* 119:193–204
- Adamides NG (2013) South Mathiatis: an unusual volcanogenic sulphide deposit in the Troodos ophiolite of Cyprus. *Appl Earth Sci* 122:194–206
- Alt JC (1994) A sulfur isotopic profile through the Troodos ophiolite, Cyprus: primary composition and the effects of seawater hydrothermal alteration. *Geochim Cosmochim Acta* 58:1825–1840
- Alt JC (1995) Subseafloor processes in mid-ocean ridge hydrothermal systems. In: Humphris SE, Zierenberg RA, Mullineaux LS, Thomson RE (eds) *Seafloor hydrothermal systems: physical, chemical, biological, and geological interactions*. *Geophys Monograph* 91, American Geophysical Union, Washington, DC, pp 85–114
- Alt JC, Shanks WC (2011) Microbial sulfate reduction and the sulfur budget for a complete section of altered oceanic basalts, IODP hole 1256D (eastern Pacific). *Earth Planet Sci Lett* 310:73–83
- Alt JC, Teagle DA (2003) Hydrothermal alteration of upper oceanic crust formed at a fast-spreading ridge: mineral, chemical, and isotopic evidence from ODP site 801. *Chem Geol* 201:191–211
- Balistreri LS, Chao TT (1987) Selenium adsorption by goethite. *Soil Sci Soc Am* 51:1145–1151
- Constantinou G, Govett GJS (1973) Geology, geochemistry, and genesis of Cyprus sulfide deposits. *Econ Geol* 68:843–858
- de Ronde CEJ, Hannington MD, Stoffers P, Wright IC, Ditchburn RG, Reyes AG, Baker ET, Massoth GJ, Lupton JE, Walker SL, Greene RR, Soong CWR, Ishibashi J, Lebon GT, Bray CJ, Resing JA (2005) Evolution of a submarine magmatic-hydrothermal system: Brothers volcano, southern Kermadec arc, New Zealand. *Econ Geol* 100:1097–1133
- de Ronde CE, Humphris SE, Höfig TW, Reyes AG, IODP Expedition 376 Scientists (2019) Critical role of caldera collapse in the formation of seafloor mineralization: the case of Brothers volcano. *Geology* 47:762–766
- Escartín J, Canales JP (2011) Detachments in oceanic lithosphere: deformation, magmatism, fluid flow, and ecosystems. *EOS, Trans Am Geophys Union* 92:31–31
- Galley A, Hannington M, Jonasson I (2007) Volcanogenic massive sulphide deposits. In: Goodfellow WD (ed) *Mineral Deposits of Canada: a synthesis of major deposit-types, district metallogeny, the evolution of geological provinces, and exploration methods*, Special publication no. 5. Geological Association of Canada, Mineral Deposits Division, pp 141–161
- Gamo T, Chiba H, Masuda H, Edmonds HN, Fujioka K, Kodama Y, Nanba H, Sano Y (1996) Chemical characteristics of hydrothermal fluids from the TAG mound of the mid-Atlantic ridge in August 1994: implications for spatial and temporal variability of hydrothermal activity. *Geophys Res Lett* 23:3483–3486
- Gass IG (1968) Is the Troodos massif of Cyprus a fragment of Mesozoic Ocean floor? *Nature* 220:39–42
- Gass IG (1980) The Troodos massif: its role in the unravelling of the ophiolite problem and its significance in the understanding of constructive plate margin processes, in: *Ophiolites, proceedings of the international Ophiolite symposium, Cyprus 1979*. The Geological Survey Department, Ministry of Agriculture and Natural Resources, Nicosia, Cyprus, pp 23–35
- Gass IG, Snewing JD (1973) Intrusion, extrusion and metamorphism at constructive margins: evidence from the Troodos massif, Cyprus. *Nature* 242:26–29
- Halbach M, Halbach P, Lüders V (2002) Sulfide-impregnated and pure silica precipitates of hydrothermal origin from the Central Indian Ocean. *Chem Geol* 182:357–375
- Hannington MD, Scott SD (1989) Sulfidation equilibria as guides to gold mineralization in volcanogenic massive sulfides; evidence from sulfide mineralogy and the composition of sphalerite. *Econ Geol* 84:1978–1995
- Hannington MD, Peter JM, Scott SD (1986) Gold in sea-floor polymetallic sulfide deposits. *Econ Geol* 81:1867–1883
- Hannington M, Herzig P, Scott S, Thompson G, Rona P (1991) Comparative mineralogy and geochemistry of gold-bearing sulfide deposits on the mid-ocean ridges. *Mar Geol* 101:217–248
- Hannington MD, Galley A, Herzig P, Petersen S (1998) Comparison of the TAG mound and stockwork complex with Cyprus-type massive sulfide deposits. *Proc Ocean Drill Program Sci Results* 158:389–415
- Heinrich CA, Driesner T, Stefánsson A, Seward TM (2004) Magmatic vapor contraction and the transport of gold from the porphyry environment to epithermal ore deposits. *Geology* 32:761–764
- Herzig PM, Hannington MD, Scott SD, Maliotis G, Rona PA, Thompson G (1991) Gold-rich sea-floor gossans in the Troodos Ophiolite and on the mid-Atlantic ridge. *Econ Geol* 86:1747–1755
- Herzig PM, Hannington MD, Arribas A Jr (1998) Sulfur isotopic composition of hydrothermal precipitates from the Lau back-arc: implications for magmatic contributions to seafloor hydrothermal systems. *Miner Deposita* 33:226–237
- Honnorez J, Von Herzen RP, Barrett TJ, Becker K, Bender ML, Borella PE, Hubberten HW, Jones SC, Karato SI, Laverne C, Levi S (1981) Hydrothermal mounds and young ocean crust of the Galapagos: preliminary deep sea drilling results, leg 70. *Geol Soc of Am Bull* 92:457–472
- Humphris SE, Cann JR (2000) Constraints on the energy and chemical balances of the modern TAG and ancient Cyprus seafloor sulfide deposits. *J Geophys Res Solid Earth* 105:28477–28488
- Humphris SE, Herzig PM, Miller DJ, Alt JC, Becker K, Brown D, Brüggemann G, Chiba H, Fouquet Y, Gemmill JB, Guerin G, Hannington MD, Holm NG, Honnorez JJ, Iturrino GJ, Knott R, Ludwig R, Nakamura K, Petersen S, Reysenbach A-L, Rona PA, Smith S, Sturz AA, Tivey MK, Zhao X (1995) The internal structure of an active sea-floor massive sulphide deposit. *Nature* 377:713–716

- Hurst SD, Moores EM, Varga RJ (1994) Structural and geophysical expression of the Solea graben, Troodos Ophiolite, Cyprus. *Tectonics* 13:139–156
- Huston DL, Large RR (1989) A chemical model for the concentration of gold in volcanogenic massive sulphide deposits. *Ore Geol Rev* 4: 171–200
- Jowitt SM, Jenkin GRT, Coogan LA, Naden J (2012) Quantifying the release of base metals from source rocks for volcanogenic massive sulfide deposits: effects of protolith composition and alteration mineralogy. *J Geochem Explor* 118:47–59
- Keith M, Haase KM, Schwarz-Schampera U, Klemm R, Petersen S, Bach W (2014) Effects of temperature, sulfur, and oxygen fugacity on the composition of sphalerite from submarine hydrothermal vents. *Geology* 42:699–702
- Keith M, Haase KM, Klemm R, Krumm S, Strauss H (2016) Systematic variations of trace element and sulfur isotope compositions in pyrite with stratigraphic depth in the Skouriotissa volcanic-hosted massive sulfide deposit, Troodos ophiolite, Cyprus. *Chem Geol* 423:7–18
- Koski RA, Clague DA, Oudin E (1984) Mineralogy and chemistry of massive sulfide deposits from the Juan de Fuca ridge. *GSA Bull* 95: 930–945
- Mamindy-Pajany Y, Hurel C, Marmier N, Roméo M (2009) Arsenic adsorption onto hematite and goethite. *C R Chim* 12:876–881
- Martin AJ, McDonald I, MacLeod CJ, Prichard HM, McFall K (2018) Extreme enrichment of selenium in the Apliki Cyprus-type VMS deposit, Troodos, Cyprus. *Mineral Mag* 82:697–724
- Martin AJ, Keith M, McDonald I, Haase KM, McFall KA, Klemm R, MacLeod CJ (2019) Trace element systematics and ore-forming processes in mafic VMS deposits: evidence from the Troodos ophiolite, Cyprus. *Ore Geol Rev* 106:205–225
- Martin AJ, Keith M, Parvaz DB, McDonald I, Boyce AJ, McFall KA, Jenkin GR, Strauss H, MacLeod CJ (2020) Effects of magmatic volatile influx in mafic VMS hydrothermal systems: evidence from the Troodos ophiolite, Cyprus. *Chem Geol* 531:119–325
- Maslennikov VV, Maslennikova SP, Large RR, Danyushevsky LV, Herrington RJ, Ayupova NR, Zaykov VV, Lein AY, Tseluyko AS, Melekestseva IY, Tessalina SG (2017) Chimneys in Paleozoic massive sulfide mounds of the Urals VMS deposits: mineral and trace element comparison with modern black, grey, white and clear smokers. *Ore Geol Rev* 85:64–106
- Melekestseva IY, Maslennikov VV, Tret'yakov GA, Nimis P, Beltenev VE, Rozhdestvenskaya II, Maslennikova SP, Belogub EV, Danyushevsky L, Large R, Yuminov AM, Sadykov SA (2017) Gold- and silver-rich massive sulfides from the Semenov-2 hydrothermal field, 13°31.13'N, mid-Atlantic ridge: a case of magmatic contribution? *Econ Geol* 112:741–773
- Mercier-Langevin P, Hannington MD, Dubé B, Bécu V (2011) The gold content of volcanogenic massive sulfide deposits. *Mineral Deposita* 46:509–539
- Miyashiro A (1973) The Troodos ophiolitic complex was probably formed in an island arc. *Earth Planet Sci Lett* 19:218–224
- Monecke T, Petersen S, Hannington MD, Grant H, Samson I (2016) The minor element endowment of modern sea-floor massive sulfides and comparison with deposits hosted in ancient volcanic successions. *Rev Econ Geol* 18:245–306
- Moss R, Scott SD (2001) Geochemistry and mineralogy of gold-rich hydrothermal precipitates from the eastern Manus Basin, Papua New Guinea. *Can Mineral* 39:957–978
- Mukasa SB, Ludden JN (1987) Uranium-lead isotopic ages of plagiogranites from the Troodos ophiolite, Cyprus, and their tectonic significance. *Geology* 15:825–828
- Naden J, Herrington RJ, Jowitt SM, Mcevoy FM, Williamson JP, Monhemius AJ (2006) New methodologies for volcanic-hosted copper sulphide mineralization on Cyprus: a GIS-prospectivity analysis-based approach. BGS internal report CR/06/129, pp 1–241
- Patten CGC, Pitcairn IK, Teagle DAH, Harris M (2016) Mobility of Au and related elements during the hydrothermal alteration of the oceanic crust: implications for the sources of metals in VMS deposits. *Mineral Deposita* 51:179–200
- Patten CGC, Pitcairn IK, Teagle DAH (2017) Hydrothermal mobilisation of Au and other metals in supra-subduction oceanic crust: insights from the Troodos ophiolite. *Ore Geol Rev* 86:487–508
- Patten CGC, Pitcairn IK, Alt JC, Zack T, Lahaye Y, Teagle DAH, Markdahl K (2019) Metal fluxes during magmatic degassing in the oceanic crust: sulfide mineralization at ODP site 786B, Izu-Bonin forearc. *Mineral Deposita* 55:469–489
- Pearce JA, Robinson PT (2010) The Troodos ophiolitic complex probably formed in a subduction initiation, slab edge setting. *Gondwana Res* 18:60–81
- Pedersen LER, Staudigel H, McLoughlin N, Whitehouse MJ, Strauss H (2017) A multiple sulfur isotope study through the volcanic section of the Troodos ophiolite. *Chem Geol* 468:49–62
- Petersen S, Herzig PM, Hannington MD (2000) Third dimension of a presently forming VMS deposit: TAG hydrothermal mound, mid-Atlantic ridge, 26°N. *Mineral Deposita* 35:233–259
- Pokrovski GS, Akinfiyev NN, Borisova AY, Zotov AV, Kouzmanov K (2014) Gold speciation and transport in geological fluids: insights from experiments and physical-chemical modelling. *Geol Soc Lond Spec Publ* 402:9–70
- Prichard HM, Malotis G (1998) Gold mineralization associated with low-temperature, off-axis, fluid activity in the Troodos ophiolite, Cyprus. *J Geol Soc* 155:223–231
- Scott SD, Barnes HL (1971) Sphalerite geothermometry and geobarometry. *Econ Geol* 66:653–669
- Sun W, Arculus RJ, Kamenetsky VS, Binns RA (2004) Release of gold-bearing fluids in convergent margin magmas prompted by magnetite crystallization. *Nature* 431:975–978
- Tivey MK, Humphris SE, Thompson G, Hannington MD, Rona PA (1995) Deducing patterns of fluid flow and mixing within the TAG active hydrothermal mound using mineralogical and geochemical data. *J Geophys Res Solid Earth* 100:12527–12555
- Urabe T, Kusakabe M (1990) Barite silica chimneys from the Sumisu rift, Izu-Bonin arc: possible analog to hematitic chert associated with Kuroko deposits. *Earth Planet Sci Lett* 100:283–290
- van Everdingen DA, Cawood PA (1995) Dyke domains in the Mitsero graben, Troodos ophiolite, Cyprus: an off-axis model for graben formation at a spreading centre. *J Geol Soc* 152:923–932
- Varga RJ, Moores EM (1985) Spreading structure of the Troodos ophiolite, Cyprus. *Geology* 13:846–850
- Von Damm KL (1995) Controls on the chemistry and temporal variability of seafloor hydrothermal fluids. *Seafloor hydrothermal systems: physical, chemical, biological, and geological interactions*. In: Humphris SE, Zierenberg RA, Mullineaux LS, Thomson RE (eds) *Seafloor hydrothermal systems: physical, chemical, biological, and geological interactions*. Geophys Monograph 91, American Geophysical Union, Washington, DC, pp 222–247
- Webber AP, Roberts S, Murton BJ, Mills RA, Hodgkinson MRS (2017) The formation of gold-rich seafloor sulfide deposits: evidence from the Beebe hydrothermal vent field. *Cayman Trough Geochim Geophys Geosystems* 18:2011–2027
- White NC, Hedenquist JW (1990) Epithermal environments and styles of mineralization: variations and their causes, and guidelines for exploration. *J Geochem Explor* 36:445–474
- Williams-Jones AE, Heinrich CA (2005) Vapor transport of metals and the formation of magmatic-hydrothermal ore deposits. *Econ Geol* 100:1287–1312

- Williams-Jones AE, Bowell RJ, Migdisov AA (2009) Gold in solution. *Elements* 5:281–287
- Yang K, Scott SD (1996) Possible contribution of a metal-rich magmatic fluid to a sea-floor hydrothermal system. *Nature* 383:420–423

Publisher's note Springer Nature remains neutral with regard to jurisdictional claims in published maps and institutional affiliations.